BUTTERWORTH HEINEMANN

Polymer Vol. 36 No. 5, pp. 921–930, 1995
Elsevier Science Ltd
Printed in Great Britain

Toughening mechanism of rubber-modified polyamides

O. K. Muratoglu*, A. S. Argon†‡ and R. E. Cohen§
**Program in Polymer Science and Technology and Department of Materials Science and Engineering, †Department of Mechanical Engineering and §Department of Chemical Engineering, Massachusetts Institute of Technology, Cambridge, MA 02139, USA*

and M. Weinberg
E.I. du Pont de Nemours & Company, Central Research and Development Department, Experimental Station, Wilmington, DE 19898, USA
(Received 13 August 1994)

Rubber-modified polyamides were probed using scanning electron microscopy (SEM), transmission electron microscopy (TEM), small-angle X-ray scattering and various mechanical tests. TEM studies showed that in tough samples the crystalline orientation in the interparticle region is of a distinctly different character. The lamellae are organized perpendicular to the rubber–matrix interface, while the hydrogen-bonded planes of low slip resistance are aligned parallel to these interfaces. Based on this observation a model is proposed to elucidate the deformation and toughening mechanisms of these materials. Further SEM studies in the stress-whitened regions of both the tensile bars and Izod specimens revealed the evolution of a cavitation process in the rubber particles. The shape and the size of the cavities in tough samples is related to the initial morphology of the matrix.

(Keywords: rubber-modified polyamides; toughening mechanism; deformation)

INTRODUCTION

Polyamides are known to be notch-sensitive engineering thermoplastics arising from a significantly lower resistance to crack propagation than crack initiation. As a consequence, polyamides are brittle at high strain rates and/or low temperatures. Modification of these semi-crystalline polymers with thermoplastic elastomers or rubbers is a commonly employed practice to counteract such embrittlement. For instance, the addition of 20 wt% ethylene propylene diene rubber in polyamide 6 increases the notched Izod toughness 20-fold when the rubber particle size is kept below 1.0 μm[1]. Previously, several studies have documented the effect of various parameters such as rubber particle size[1,2], rubber concentration[1] and interparticle distance[3] on the toughening efficiency of such rubber modifiers. From these studies it has been established that for the blend to be tough, the particles should be smaller than a critical size that depends on the rubber concentration. Similarly, the rubber concentration should be above a critical level which is a function of the particle size. Wu[3] considered these two interdependent parameters in combination in the form of a single parameter, namely, the interparticle distance (D_i). Based on the assumption of a lattice-like packing of uniform sized particles, Wu has calculated the interparticle distance using the following relation:

$$D_i = d[(\pi/6\phi_r)^{1/3} - 1] \quad (1)$$

where ϕ_r is the rubber concentration and d is the rubber particle diameter. This relation provides a rough estimate for D_i, in that variations through which the spatial and size distributions of the particles, and possible occlusions of polyamide inside the particles, affect the assumptions involving lattice-like packing of uniform-sized particles.

Wu's observations on a rubber-modified polyamide 66 demonstrated that regardless of particle size and rubber concentration, the blends are toughened if the D_i is $<0.3\,\mu$m. Several attempts have been made to identify the mechanism behind this critical transition phenomenon[3,4] and some models[3–8] have been proposed.

Thus, Wu proposed first, that strong overlap of the stress fields around the particles induces shear yielding and crazing of the matrix, thereby toughening the polyamide 66/rubber blends[4]. In later work however, Wu recognized the inadequacy of this model in explaining the particle size effect on toughening[3], since the local stress level in an inclusion-filled matrix is only a function of the ratio of the centre to centre distance (L) to the diameter of the particle (d). This ratio remains constant at a given volume fraction of particles regardless of their size. Therefore, according to the stress field overlap model, toughening should be unaffected by the presence of large particles at any given L/d ratio. This is contradictory to the experimental results which show clearly that smaller particles are more effective in toughening[1].

In another attempt to offer an explanation of this effect, Wu proposed a second model which is based on the stress-state transition at the critical D_i. In this model[3], it is stated that as the particle density increases and the D_i goes through the critical value, the material in this region transforms from a state of plane strain to plane stress. As a consequence, the deformation resistance of these regions decreases and the blend becomes tough. However, a differentiation of local stress state between plane stress or plane strain has no meaning in this context.

‡To whom correspondence should be addressed

The model indirectly attributes the embrittlement to the presence of high triaxial stresses. Once again, the presence or the absence of triaxial stresses in local regions between particles can be affected only by changes in geometrical ratios, which remain constant at a given volume fraction and geometrical dispersion of particles regardless of their size. Thus, such an argument is unacceptable, leaving the explanation at a true size-dependent material property rather than stress state, or any other characteristic of a deformation field.

Currently available explanations of the toughening effect of rubbery inclusions in polyamide matrices are ambiguous and require clarification. The present study takes a new approach to explore this toughening mechanism by examining the changes in the matrix morphology (crystallographic texture) induced by the second phase particles. This is based on detailed examinations by the present authors of the crystalline texture in thin films of polyamide 6 which established that the (001) (presumably lowest energy) planes of polyamide 6 containing the hydrogen bonds preferentially align parallel to a rubbery/polyamide interface[9]. Based on this observation, the rubber–matrix interface in a toughened polyamide is believed to similarly influence the crystallization behaviour of the matrix. In the present study we discuss these morphological changes in a similar matrix (polyamide 6) using our observations on polyamides modified with ethylene propylene diene rubber grafted with maleic anhydride (PA 66/EPDR-*g*-MA). We also relate these crystallographic textures in the polyamide to the morphologies observed after the deformation of these blends. Since the (001)[010] system in polyamide 6 is known to have by far the lowest slip resistance[10], a definite material-specific explanation of the toughness transition becomes possible.

EXPERIMENTAL

Sample preparation

The blends of polyamide 66 and ethylene/propylene anhydride-functionalized rubber were prepared in a 28 mm Werner and Pfleiderer extruder. The rubber weight fractions and functionality levels were independently varied. The resulting pellets were moulded in a 6 oz, 150 ton Van Dorn injection moulding machine into dog-bone tensile bars (gauge length = 100 mm, width = 12.5 mm, thickness = 3.2 mm) and flexural test bars (127 mm long, width = 12.5 mm, thickness = 3.2 mm). The flexural bars were then divided into two 63.5 mm long pieces, one close to the gate and the other far from the gate. Notches were cut into each part with a TMI Notching Cutter according to the specifications of ASTM D256.

Particle size determination

The particle sizes of the PA 66/EPDR-*g*-MA have been determined using two complementary techniques: microscopy and scattering. The experimental procedure for particle size determination using scanning electron microscopy (SEM) is explained later. Small-angle X-ray scattering (SAXS) is particularly useful for accurately determining rubber particle sizes in moulded parts because of the large electron density difference between the polyamide and the rubber. In addition, SAXS scans $\sim 10^{12}$ particles *versus* $\sim 10^{2}$ particles in transmission electron microscopy (TEM). Here, an ultra-high resolution diffractometer (Bonse-Hart) was used to allow resolution of particles $< \sim 800\ \mu m$ in diameter. To obtain size information, the scattering results were modelled with a log-normal distribution of independent spherical particles. Analysis of the invariant (the intensity times the square of the scattering angle) leads to a size distribution characterized by its median and a breadth factor[11]. Because the method gives a weight-average particle size, its values are generally slightly higher than those obtained from TEM images.

Transmission electron microscopy

The PA 6/EPDR-*g*-MA samples of various particle size and rubber concentration were dissolved in trifluoroethanol to prepare 2 wt% solutions. Thin films of 0.5–1.0 μm thickness were spin coated from these solutions on a polystyrene (PS) coated polished silicon substrate. The PS layer was then dissolved in a toluene bath to transfer the polyamide films onto copper TEM grids. The samples were annealed in a brass vacuum chamber immersed in an oil bath at 230°C for 4 h, in order to remove the orientation, induced through the spinning process. Following the method of Martinez-Salazar[12], an aqueous solution of 2 vol% phosphotungstic acid (PTA) and 2 vol% benzyl alcohol was prepared to stain the thin films to reveal the lamellar microstructure. Staining was carried out at room temperature by immersing the films in the PTA solution for 15 min. The samples were then washed in distilled water. A Jeol 200CX transmission electron microscope was operated at 100 kV accelerating voltage to record the morphology in the bright field mode.

Mechanical testing

Dog-bone tensile specimens of PA 66/EPDR-*g*-MA prepared as described earlier, were tested in an Instron 4200 testing machine at an initial strain rate of $1\ s^{-1}$. The Izod tests were conducted on dry-as-moulded samples according to ASTM D256. The results in *Table 1* are the averages of tests from the 'far' end of the bars. The samples were not conditioned prior to testing to remove the water and eliminate its effect on mechanical properties. Rather, all samples were handled according to exactly the same procedures prior to testing to ensure that they all contained essentially the same concentration of water. Immediately after injection moulding, the samples had been put in air-tight bags under dry nitrogen and kept in a desiccator until they were tested. It is known from earlier experiments[13] that complete removal of water from thick polyamide specimens is virtually impossible, nor is this desirable since it results in a very brittle and irrelevant material. Through a comparison of the results of the present study with that of Galeski *et al.*[14], we estimate the water content of our material to be ~ 1.0 wt%.

Scanning electron microscopy

SEM was performed on an Electroscan environmental scanning electron microscope (ESEM) with a cerium hexaboride filament. This microscope operates under an adjustable vapour pressure in the range of 0.1–10 torr. This moist environment can prevent electron charging on insulating surfaces. Although charging of the sample was not an issue, a very thin discontinuous coating of

Table 1 Mechanical properties of the PA 66/EPDR-*g*-MA samples used in tensile and notched Izod tests

	Sample code	EPDR-*g*-MA conc. (wt%)	SEM particle size (nm)[a]	SAXS particle size (nm)[b]	Notched Izod ($J\,m^{-1}$)	Yield stress (MPa)	Strain to failure (%)
Constant rubber concentration	98-0	0	–	–	–	82	22.39
	98-1	19	28 000	>800	69	–	1.96
	98-2	19	1500	>800	213	50	14.70
	98-3	19	1420	>800	752	50	32.50
	98-4	19	720	715	876	50	50.00
	98-5	19	350	349	1099	50	67.10
	98-6	19	250	252	1191	45	97.40
Constant particle size	98-7	6	240	232	75	76	28.62
	98-8	10	250	255	224	65	34.15
	98-9	12	230	248	966	60	40.13
	98-10	14	250	254	939	57	48.14
	98-6	19	250	252	1191	45	97.40

[a] Number-average particle size
[b] Weight-average particle size

Au or Au/Pd was applied to improve the resolution of the microscope.

To measure the particle size, undeformed rubber-modified polyamide 66 tension specimens were cryo-fractured perpendicular to the flow direction in the mould. These surfaces were then gold coated and micrographs were recorded in the ESEM. The cavitation in the bulk of the deformed samples was also studied. This was done by cryofracturing the broken tensile bars and Izod flex bars along different directions. *Figure 1* shows a schematic illustration of the cryofracturing process for both the Izod bar and tensile specimens: IZOD1 and IZOD2 type cryofracturing exposed the internal structure of the cavities in the intensely deformed regions near the crack flanks in planes parallel and perpendicular to the line of the crack tip, respectively, while TENS1 direction provided surfaces with a lateral view of the cavities formed during deformation. The tensile bars were fractured only along the tensile axis because the orientation induced during testing does not permit successful cryofracturing perpendicular to the loading direction. The cryofracturing is performed as follows: a notch is introduced along a desired direction and the sample is left in liquid nitrogen for 20 min. A wedge is then driven into the notch to cleave the specimen while it is still at liquid nitrogen temperature. The exposed internal surfaces were then gold-coated and examined under ESEM at an accelerating voltage of 15 kV.

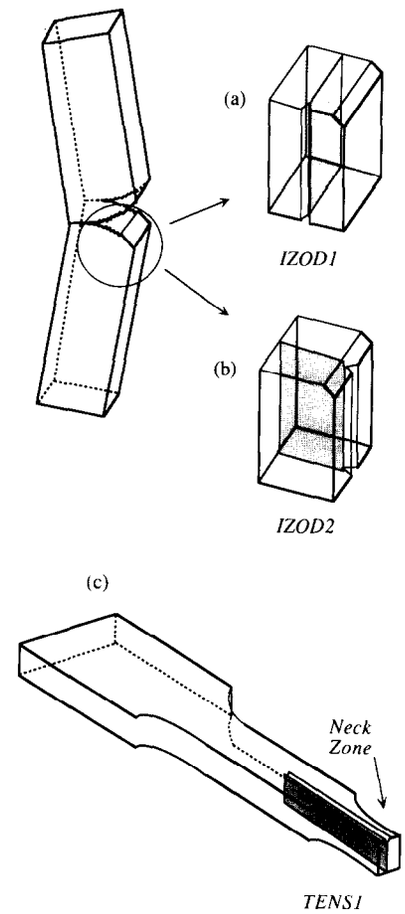

Figure 1 Cryofracturing of the deformed samples. The shaded surfaces were exposed for microscopy by cryofracturing along the indicated notch: (a) IZOD1 view; (b) IZOD2 view; (c) TENS1 view

RESULTS AND DISCUSSION

Our recent study[9] of thin films of polyamide 6 sandwiched between EPDR layers, demonstrated that upon melt crystallization, the (001) crystallographic planes containing the hydrogen bonds preferentially align themselves parallel to the rubber–polyamide interface. This orientation is prevalent in films thinner than 0.15 μm. The reciprocal lattice vector **c*** is normal to the film plane and the direct lattice vectors **a** and **b** are randomly oriented in the plane of the film. In relatively thicker films, the average preferred orientation degrades and approaches a random texture, while a thin oriented surface layer of a submicrometre thickness always remains. It was postulated that the preferred orientation of low energy hydrogen-bonded planes parallel to the interface serves to minimize the interfacial energy and that this effect has a penetration depth of the order of 100 nm. In films of a thickness in the range of 0.1–0.2 μm,

the influence of the top and bottom interfaces overlaps and the film assumes a preferred orientation throughout. In thicker films the two interfaces move apart and the overlap is not possible, while other random lamellar orientation fill-in between the two interface layers, leaving the film as a whole approaching a random orientation.

Matrix morphology in the interparticle region

The above-mentioned discovery of preferred orientation of hydrogen-bonded planes near rubber–polyamide interfaces led to the present investigation of the matrix morphology in rubber-modified polyamides. Unlike the earlier study where the interface is planar[9], in a rubber-modified polyamide system the particles are spherical in shape and the interface has a finite curvature. To determine the local orientation of the polyamide crystals near the interface, TEM was utilized. The crystalline texture had to be preserved during sample preparation. Therefore, microtoming methods were not used since these can induce very large orientational changes during the microtoming process where shear strains of the order of 200–300% can destroy the crystalline texture. Instead, thin films of 0.1–0.2 μm thickness were directly prepared via spin coating as explained in the Experimental section. *Figure 2* shows the morphologies observed in thin films of polyamide 6 modified with EPDR-*g*-MA. The contrast is achieved by staining the films with PTA. When the thin films are immersed in the aqueous solution of PTA and benzyl alcohol, benzyl alcohol penetrates and swells the amorphous regions, locally enhancing the diffusion of WO_3 which we have determined is the penetrating species in PTA staining. Therefore, the dark zones are the amorphous regions and the bright lines represent the crystalline lamellae. The stain does not penetrate the rubbery phase leaving these regions on the bright side of the contrast.

As *Figure 2* shows, the lamellae are randomly oriented in the bulk of the matrix. Around some of the particles the morphology of the matrix appears at first sight to be unaffected. A closer perusal, however, shows a prevalence of lamellae impinging on particle interfaces along radial directions. In particular, the interparticle regions of closely spaced particles exhibit a different morphology. That is, the lamellae are organized parallel to each other and perpendicular to the rubber–matrix interface. One possible path of reaching this morphology could be through the nucleation of the lamellae near the particle–matrix interface. Assuming that this nucleation process has come about, the hydrogen-bonded planes should become oriented parallel to the interface for energetic reasons which should also govern the free energy of formation of crystal nuclei: the crystallization of polyamides occurs by the formation of one hydrogen-bonded sheet at a time[15] which implies that the normals to these planes constitute the direction of rapid growth. Once nucleation of the oriented lamellae occurs near the particles, the growing face of the lamellae, i.e. the hydrogen-bonded planes, should remain parallel to the interface. This hypothesis is consistent with our previous observations which closely demonstrated that the hydrogen-bonded planes of polyamide 6 align parallel to a planar rubber–polyamide interface[9]. The proposed orientation of the crystalline planes with respect to the interface can be confirmed through selected area electron diffraction. Unfortunately, the crystalline state in the films degrades too rapidly under the electron beam to permit the examination of the short-lived diffraction patterns.

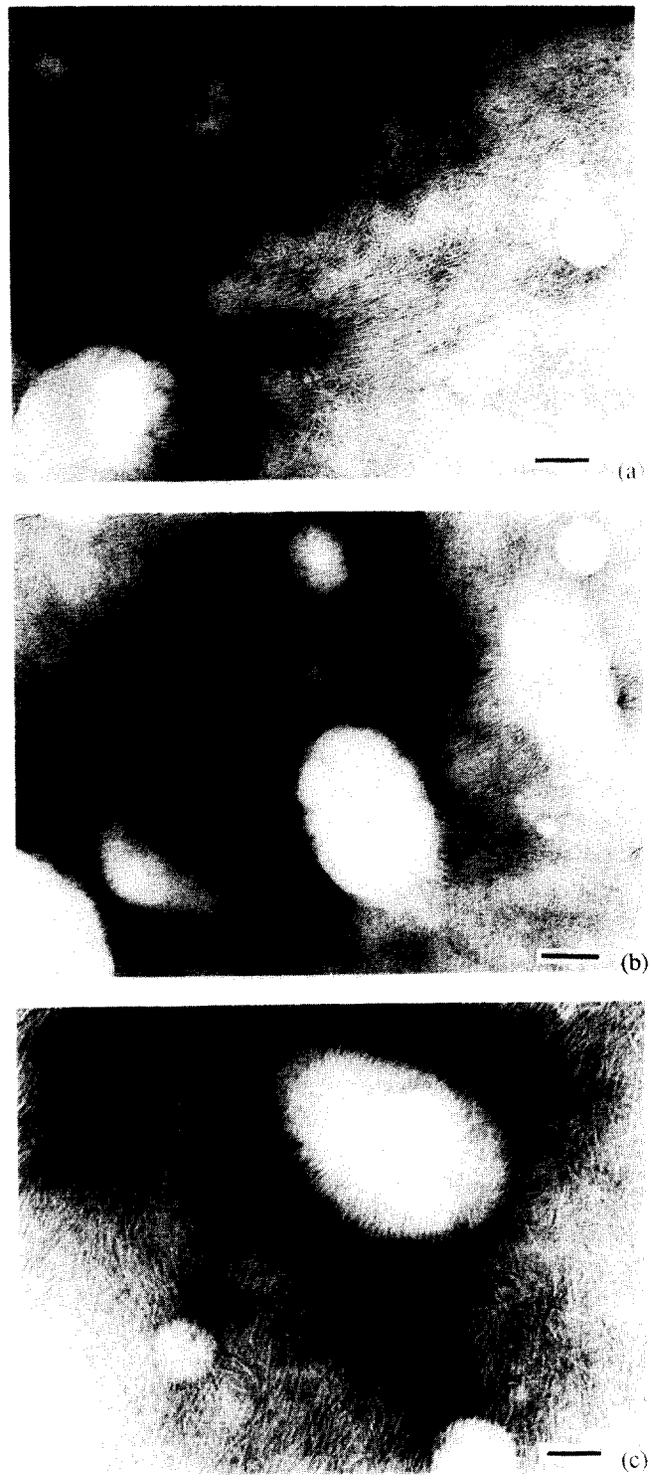

Figure 2 TEM micrographs of different regions in a polyamide 6 modified with EPDR-*g*-MA: (a) and (b) are taken at low magnification and (c) at high magnification. The sample was negatively stained with phosphotungstic acid. The dark lines are the amorphous regions and the white lines are the lamellae. The rubber particles are not stained and appear white. The scale bars represent 200 nm in (a) and (b) and 100 nm in (c)

It is not clear from TEM micrographs whether or not the crystallization of the lamellae starts from the interface. Around most of the closely spaced particles, the morphology suggests a near interface nucleation

process. However, some of the particles are surrounded by randomly oriented lamellae and most exhibit the preferred orientation in certain regions around the interface. The interpretation of these ambiguities is beyond the scope of this study and will not be discussed here. However, we use the observed morphology, and based on the preferred organization of lamellae in the interparticle regions of tough samples, we propose the following model to elucidate the local plastic deformation and toughening mechanisms of rubber-modified polyamides.

Toughening and deformation mechanisms

The deformation behaviour of semicrystalline polymers is strongly dependent on the crystalline orientation[10,16]. Consequently, tough specimens where interparticle regions retain local preferred orientation would possess a strong local mechanical anisotropy. With these findings, it is possible to construct a unique model of deformation in rubber-modified polyamides. We propose a local anisotropy model where the blended system is considered to be made up of three distinct regions: (1) low modulus rubber particles; (2) oriented interparticle region; and (3) bulk matrix. *Figure 3* illustrates a schematic rendering of the morphology and the proposed model with parallel lines indicating the oriented lamellae. For clarity, the randomly oriented lamellae of the bulk are not shown. The interparticle region is the distinctive feature between brittle and tough specimens: for the former, the region between the particles would maintain a substantially random orientation of the crystals, while the latter would have a preferred orientation of hydrogen-bonded planes parallel to the rubber–matrix interface. The bulk matrix, away from the fringing layer around the particles, on the other hand, has a randomly oriented crystalline morphology; therefore, it can be treated as an isotropic material.

Lin and Argon[10] showed that the hydrogen-bonded planes of polyamides have the lowest slip resistance. As a consequence, in tough samples the local deformation around the particles would strongly depend on the resolved shear stress on these planes. For instance, *Figure 4a* shows seven rubber particles reinforcing a matrix in an idealized packing. The parallel lines represent the intersection of the lamellae with the plane of the paper. The hydrogen-bonded planes are perpendicular to the lamellae. Therefore, in the polar extremes of the particle, with

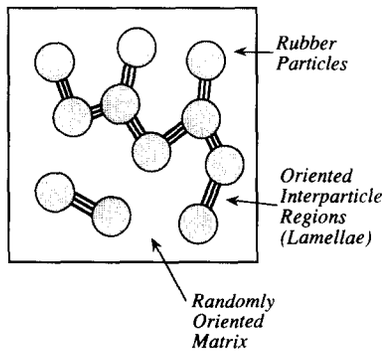

Figure 3 Schematic diagram of the proposed model and the idealized morphology of the rubber-modified polyamide system. The parallel lines between the particles are the lamellae. The randomly oriented lamellae of the matrix are left out for clarity

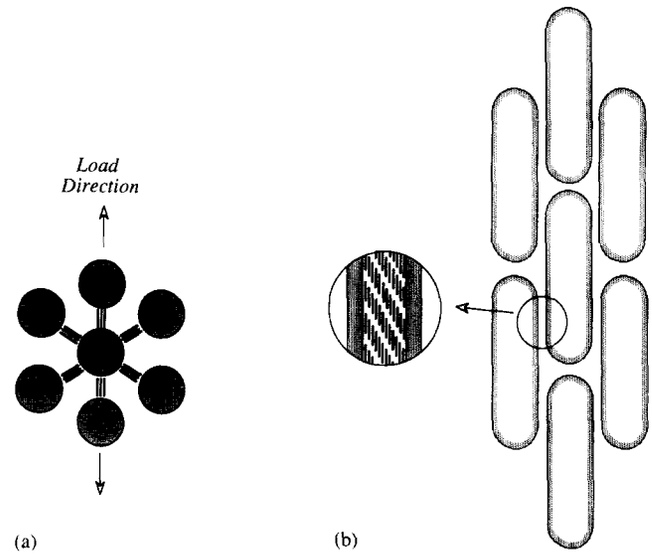

Figure 4 Schematic diagram for the deformation mechanism of an idealized morphology under uniaxial tensile test: (a) before and (b) after deformation. In (a) the parallel lines represent the intersection of lamellae with the plane of the paper while in (b) the lines in the enlarged region represent that of the hydrogen-bonded planes

reference to the direction of the applied load, the resolved shear stress on these planes is zero, and slip preferentially occurs in other high resistance slip systems resulting in small or no deformation. On the other hand, the resolved shear stress on the meridional hydrogen-bonded planes is finite and slip is likely to occur on these low resistance planes. *Figure 4b* shows the expected shape change of this simple model upon application of a uniaxial tensile stress: the rubber particles cavitate in response to the deformation-induced build-up of negative pressure in them, and the surrounding aligned crystalline regions shear to result in the pattern shown. Upon cavitation, the rubber withdraws towards the matrix to which it is strongly adhered and coats the inside surface of the cavity. The interparticle regions deform mostly by crystalline slip and some required deformations in the amorphous component. At the same time the crystals undergo lattice rotation. The insert of *Figure 4b* shows the expected crystalline morphology in the ligaments where the parallel lines represent the intersection of hydrogen-bonded planes with the plane of the paper.

According to this model, the yield stress should be lowered in regions of easy shear. This local softening phenomenon should then reduce the overall flow stress of the material allowing it to deform to large strains without initiating any critical fracture process, thus enhancing its toughness. Wu's observation of a critical D_i in rubber-modified polyamides[3] can also be rationalized by this model. When the effective D_i is below the critical value, the entire sample would behave tough through the percolation of the favourably oriented interparticle regions through the specimen. On the other hand, percolation of the readily deformable material would not be achieved in brittle samples where the particles are sparsely distributed—with much of the background matrix being randomly oriented, having a high deformation resistance.

Stress whitening and morphological features

To provide a test of the above proposed model, tensile dog-bone specimens and Izod bars with various particle

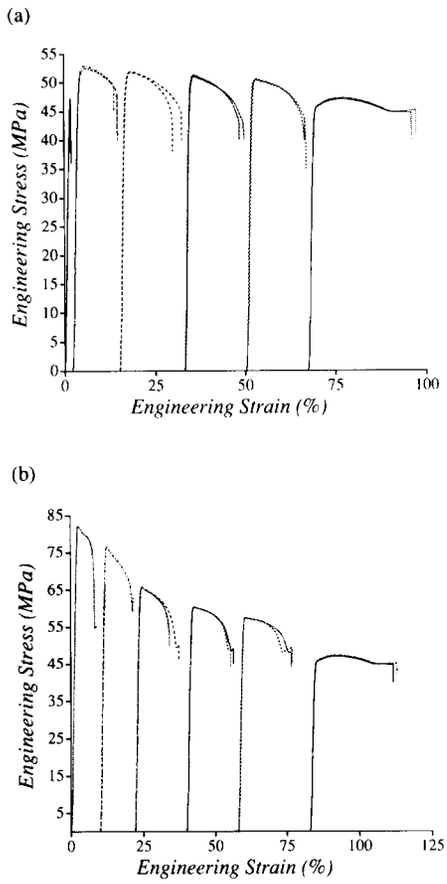

Figure 5 Tensile test results of rubber-modified polyamide 66 at (a) constant rubber concentration with particle size decreasing from left to right as 28, 1.5, 1.42, 0.72, 0.35, 0.25 μm and at (b) constant particle size with rubber concentration increasing from left to right as 0, 6, 10, 12, 14, 19 wt%. The curves are shifted for clarity

size and rubber concentration were prepared. *Table 1* summarizes the sample characteristics as well as various mechanical properties of different blends used in the tensile and notched Izod tests. *Figure 5a* shows the tensile test results at constant rubber concentration of 19 wt% and varying particle size. Similarly, *Figure 5b* represents the stress–strain behaviour of samples at constant particle size of 250 nm at varying rubber concentrations. The strain to failure increases while the yield stress decreases with increasing rubber concentration and decreasing particle size.

The deformation induced during the tensile and Izod tests creates stress-whitened regions in the samples. The tensile bars start to whiten once the stress in the gauge section of the specimen reaches the yield point. The samples that are tough at high strain rates (Izod) form a stable neck and undergo cold drawing under the low strain rate tensile test. Within the neck zone, the whitening becomes more intense. The neck travels along the gauge length of the sample and eventually fracture occurs as a critical size imperfection is acquired by the widening neck region. In like manner, tough Izod bars whiten around the fracture surface, while the brittle ones do not exhibit any whitening. In the super-tough region, the Izod specimen does not break. The crack in the sample propagates with a substantial plastic process zone at its tip as the sample bends sufficiently to permit the pendulum to swing by.

To explore the evolution of the stretch-induced morphology change in these blends during deformation the samples were cryofractured in various modes as outlined in the Experimental section. *Figures 6a* and *b* show the stress-whitened TENS1 view of an unmodified (no rubber) tensile bar after fracture outside and inside the neck zone, respectively. *Figure 7* is recorded from the TENS1 view of sample 98-2 to capture the cavitation of the rubber particles that were well bonded to the matrix by a grafting agent. In contrast, the debonding process in sample 98-1 with no grafting agent is shown in *Figure 8*. The widespread cavitation of particles in the stress-whitened region of sample 98-4 is shown in *Figures 9a*

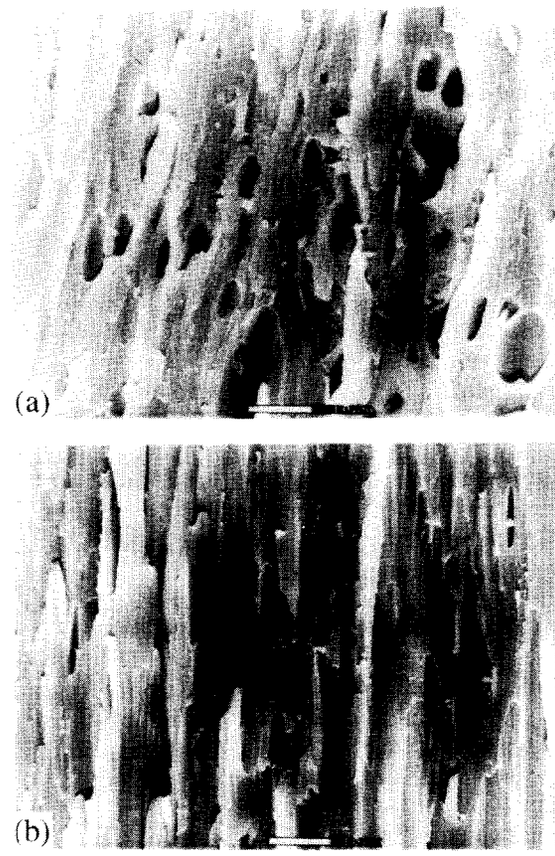

Figure 6 TENS1 view of homopolyamide 66 after uniaxial tensile test: (a) from the stress-whitened zone outside the neck region; (b) from the stress-whitened zone inside the neck region. The scale bars represent 10 μm

Figure 7 Cavitation of two rubber particles in a rubber-modified polyamide 66 recorded from the stress-whitened zone of TENS1 view of sample 98-2 after uniaxial tensile test. The scale bar represents 2 μm

Figure 8 Debonding of rubber particles from the polyamide 66 matrix in sample 98-1 with no grafting agent. The scale bar represents 50 μm

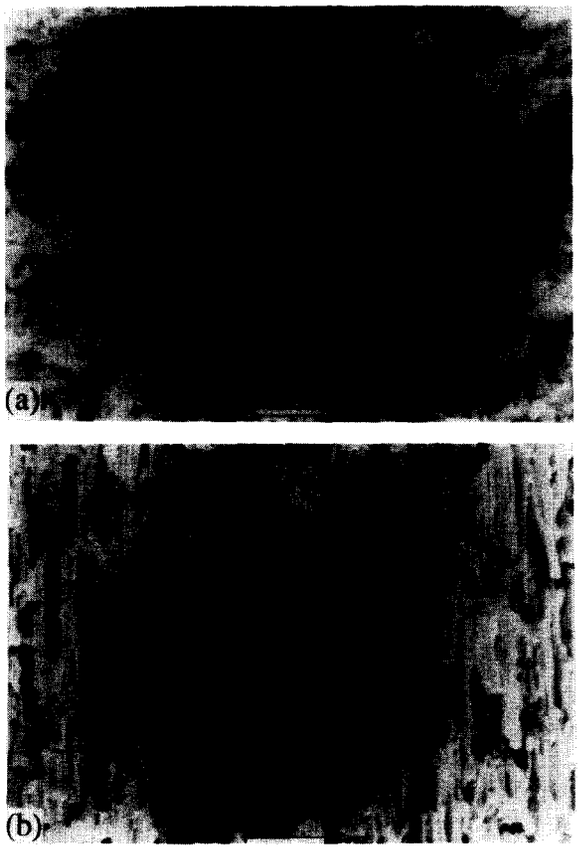

Figure 9 TENS1 view of polyamide 66 modified with 19 wt% rubber after uniaxial tensile test of sample 98-4: (a) from the stress-whitened zone outside the neck region; (b) from the stress-whitened zone inside the neck region. The scale bars represent 5 μm

and *b* recorded from the TENS1 view outside and inside the neck zone, respectively. The series of micrographs shown in *Figure 10* are recorded from the IZOD1 view of sample 98-5. *Figure 11* shows the IZOD2 view of the same sample. The above micrographs are mostly recorded from the stress-whitened regions of ductile or semiductile (within the brittle–ductile transition region) specimens. The brittle samples did not show any stress whitening around the fracture surface resulting in featureless micrographs in IZOD1 and IZOD2 views. Therefore, the micrographs of brittle samples are not shown here.

Figure 6 indicates that the stress whitening in homopolyamide 66 is due to bulk cavitation from intrinsic plastic inhomogeneities, with the cavity size ranging from 5 to 10 μm outside the neck zone. In the same sample, the cavities inside the neck region are narrower with an average width of 1 μm and are far more elongated. Upon rubber modification the cavitation process changes entirely. In this case cavitation occurs almost exclusively in and around the rubber particles while the matrix stays intact. The fracture of samples that are in the brittle–ductile transition region occurs at the early stages of the cavitation process. Therefore, cavitating particles could only be captured in these samples (e.g. 98-2) within the stress-whitened region. *Figure 7* is an example of cavitation in rubber particles of sample 98-2 where the particles were well adhered to the matrix. The morphology of the particle plays an important role in this process. Ban and co-workers[17] showed that the particles formed in these blends are composite in nature, containing as much as 40 vol% trapped polyamide occlusions. These occlusions in the rubber particles are the most likely sites of initiation of cavities. In fact, the fibrils seen inside the cavity shown in *Figure 7* are likely to have arisen from the rubber surrounding the polyamide occlusions.

The cavitation of the rubber particle is only possible if the interface between the rubber and polyamide matrix is strong enough. Otherwise, the blend is brittle and debonding of the interface occurs at low strains, where any one of the larger rubber particles can act as the fracture initiating flaw. The strength of the interface that governs the particle size effect in toughening depends on the amount of grafting between the rubber and polyamide[18]. *Figure 8* demonstrates the extensive debonding of the rubber–matrix interface in a brittle sample (98-1) with no grafting agent (maleic anhydride). The average particle size is around 28 μm and no internal cavitation of the rubber particles is discernible in the morphology, suggesting also an absence of occluded polyamide particles inside the larger rubber particles.

In tough samples where the interface is strong enough the cavitation process is abundant and occurs in almost all particles resolved by SEM. *Figure 9a* shows an example of cavitation in a sample (98-4) containing 19 wt% rubber. This micrograph is the TENS1 view outside the neck zone of a fractured tensile specimen. The cavities are uniformly distributed throughout the polyamide matrix. Unlike the spherical cavities nucleated in this region, *Figure 9b* shows elongated cavities in the neck zone. Although the average width of the cavities remains the same after necking, the cavities elongate to an average aspect ratio of 8. Hence the deformation of the cavity proceeds in such a way as to produce strain only in the direction of the applied tensile stress. Simultaneously, the matrix undergoes large strains (800%) by forming thin ligaments between the elongated cavities. Under similar conditions homopolyamide 66 failed at a strain level of 22.4% (*Figure 5a*). Exhibiting such dissimilar responses to deformation, the mechanical properties of the matrix in the interparticle region of a tough specimen should be entirely different to that of the bulk polyamide 66. In fact, as mentioned above, the interparticle region preserves an altogether different morphology that imparts distinct mechanical properties to this region. Therefore, our observation of elongated cavities supports the prediction from the model shown in *Figures 4a* and *b*.

The stress whitening around the fractured notch of tough Izod bars was also examined through cryofrac-

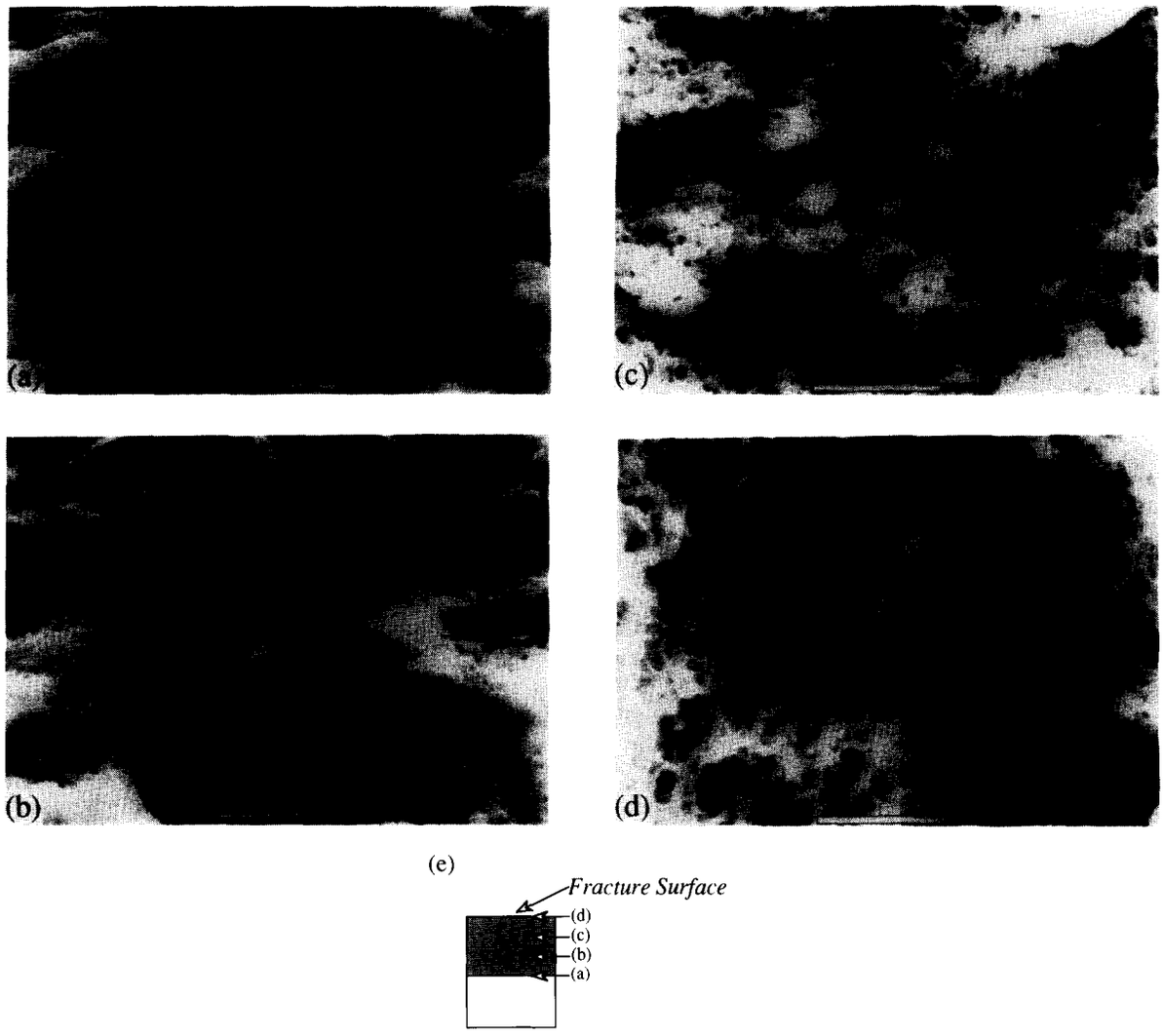

Figure 10 IZOD1 view of sample 98-4 taken inside the stress-whitened zone near the fracture surface. The location of each micrograph with respect to the fracture surface is indicated in (e) where the shaded area is the stress-whitened region. The scale bars represent 5 μm

turing in different directions as explained in the Experimental section. *Figures 10a–d* represent the IZOD1 view while *Figures 11a–d* show the IZOD2 view of sample 98-4. In both *Figures 10* and *11*, the micrographs have been recorded to capture the evolution of cavities at different depths in the stress-whitened zone away from the crack flanks. *Figure 10e* shows approximate locations of the micrographs with respect to the fracture surface. To demonstrate the significant changes in cavity size, all micrographs have been recorded with the same magnification.

The initial particle size in the sample depicted in *Figures 10* and *11* was around 250 nm. Near the fracture surface, the particles cavitated and grew to an average diameter of 1500 nm, with actual aspect ratios achieving levels of 6–8, indicating that the matrix had to undergo a strain of 600–800% before failure. This supports our model which allows the matrix to deform to large strains by locally lowering the flow stress through the initial preferred orientation of the easy shear planes around the particles in the matrix ligaments. The shape of the cavities in Izod samples is similar to that of the tensile bars. The lateral view (IZOD2, *Figure 11*) of cavities in the Izod bar and the elongated cavities of the tensile bar shown in *Figure 9b* both suggest a cylindrical-shaped cavity. In both samples, the axis of the cylinders is aligned parallel to the principal strain direction.

Another aspect of the elongated cavities in the stress-whitened regions of both the tensile and Izod specimens is that the width of the cavities does not vary during elongation. That is, the mean particle size of the specimens is almost the same as the mean width of the elongated cavities after deformation. While the cavities and the matrix ligaments elongate up to 800% strains, little or no deformation occurs in the polar regions of the cavities. The matrix in these regions undergoes almost no deformation. This observation is consistent with our model and the schematic illustration of the deformation shown in *Figures 4a* and *b*. It is important to emphasize the different nature of sampling the deformed material in the whitened zone by the IZOD1 and IZOD2 modes of sectioning. As *Figures 11a–d* show, there are fundamental rotations of the principal axes of stretch of the cavitated microstructure as a crack progresses through it. The principal axes of stretch near the fracture surface are aligned much more nearly parallel to the crack flank. This is revealed fully in the IZOD2 section while the IZOD1 section takes an oblique cut through these

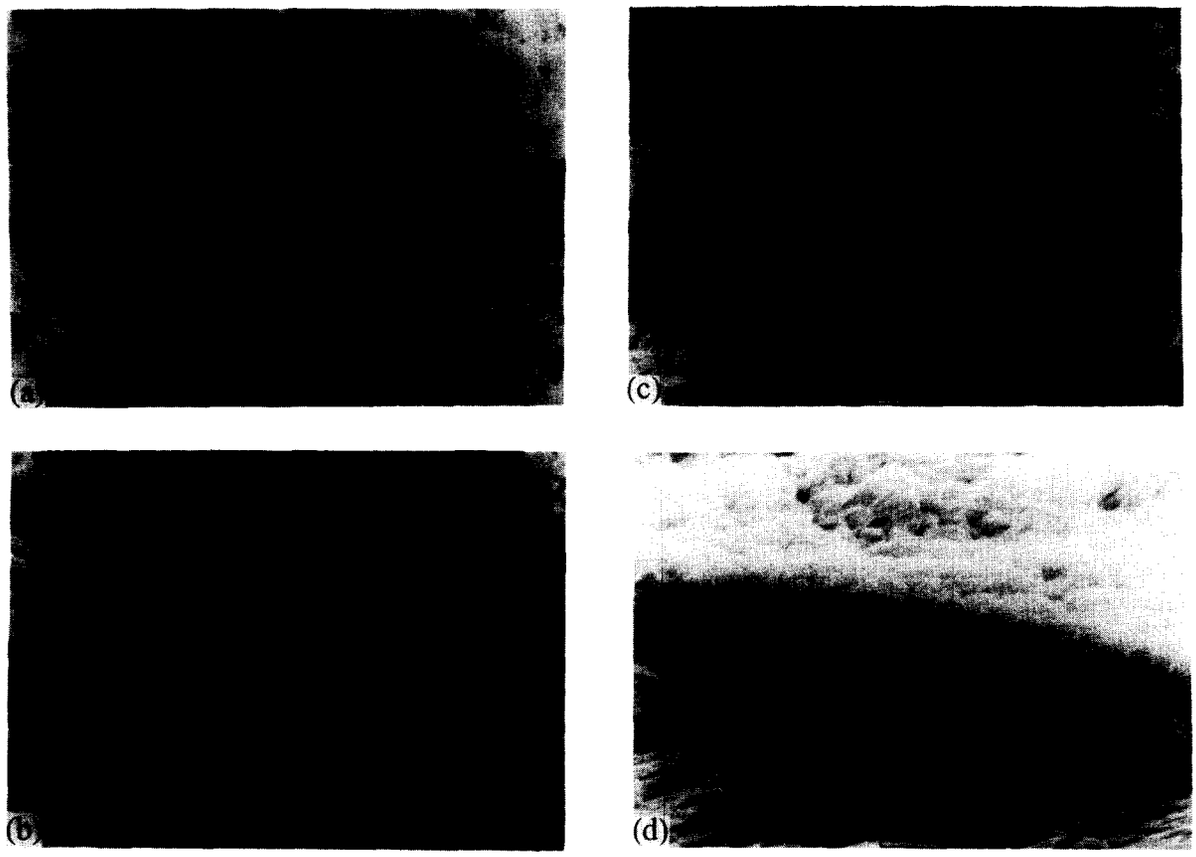

Figure 11 IZOD2 view of sample 98-4 taken inside the stress-whitened zone near the fracture surface. The location of each micrograph with respect to the fracture surface is indicated in *Figure 10e*. The scale bars represent 5 μm

elongated and rotated cavities. These important features of how the cavitated material is strained by a propagating crack will be the subject of a future paper.

From the above observations one can summarize the deformation behaviour of rubber-modified tough polyamides (with interparticle ligament thickness <0.3–$0.5\,\mu$m) as shown in *Figure 12*. Initially, the response of the material is elastic. In a tensile test, the sample starts to cavitate inside the rubber particles around the yield point. In the post-yield region of extensive plastic stretch the matrix undergoes large deformations and the cavities elongate in the direction of the applied stress (also directions of principal stretch). Thin ligaments form between the cavities as the deformation progresses resulting in fine fibrillation of the matrix. Eventually, the fibrils reach the ultimate draw ratio and fail from some inhomogeneity. Similarly, in an Izod test, the crack propagation incorporates undeformed material into the process zone, each time repeating the stages shown in *Figure 12*. Failure of the fibrils in this case represents an intrinsic property of the cavitated and stretched microstructure. Each fibril breaks upon reaching the limiting draw ratio of the matrix material. This fracture mechanism is currently under investigation. In the brittle samples with interparticle ligament thicknesses well above the critical threshold of ~ 0.3–$0.5\,\mu$m, the overall deformation resistance remains high and fracture is precipitated prematurely from a non-characteristic impurity particle or structural flaw before much overall plastic stretch can take place.

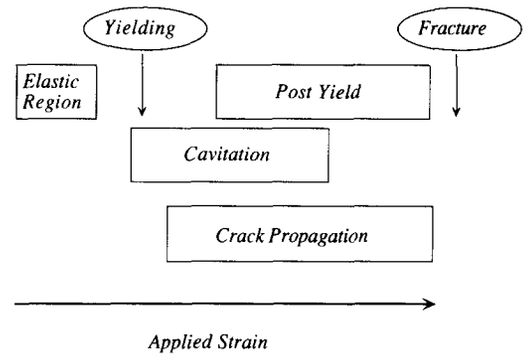

Figure 12 Schematic diagram of the deformation mechanism in rubber-modified polyamides

CONCLUSIONS

Rubber-modified polyamides go through a brittle to tough transition at a critical D_i[1,4]. This phenomenon is related to the changes in the matrix morphology induced by the rubber–matrix interface as the D_i is varied. Brittle samples have a sparse distribution of the rubber particles with large interparticle spacings (well above 0.3–0.5 μm). Therefore, the influences of the interfaces do not overlap and the matrix morphology is substantially random. On the other hand, in a tough sample where the particles are closer to each other, there is overlap of the interface-induced orientation of the crystalline morphology. This

results in a substantial fraction of material with preferred orientation of hydrogen-bonded planes parallel to the rubber–matrix interface in the interparticle zone, as indicated by clearly discernible perpendicular alignment of lamellae around the particles in TEM studies. The low slip resistance of these planes and their preferred orientation has been related to the toughening mechanism and a model has been proposed. The principal element in the proposed model is the local reduction of the flow stress that results in the hindrance of premature fracture from inevitable entrapped inorganic impurities. The morphological features observed in the stress-whitened zones of various blends are in support of this model. The chart presented in *Figure 12* summarizes stages of the deformation behaviour in rubber-modified polyamides.

ACKNOWLEDGEMENTS

This research was supported by NSF/MRL, through the Center for Materials Science and Engineering at MIT under grant no. DMR-90-22933 and by a DuPont Graduate Fellowship for OKM for which we are grateful to Dr D. Huang of the DuPont Co.

REFERENCES

1 Borggreve, R. J. M., Gaymans, R. J., Schuijer, J. and Ingen Housz, J. F. *Polymer* 1987, **28**, 1489
2 Margolina, A. and Wu, S. *Polymer* 1988, **29**, 2170
3 Wu, S. *J. Appl. Polym. Sci.* 1988, **35**, 549
4 Wu, S. *Polymer* 1985, **26**, 1855
5 Flexman, E. A. *J. Polym. Eng. Sci.* 1979, **19**, 564
6 Bucknall, C. B., Heather, P. S. and Lazzeri, A. *J. Mater. Sci.* 1989, **16**, 225
7 Hobbs, S. Y., Bopp, R. C. and Watkins, V. H. *J. Polym. Eng. Sci.* 1983, **23**, 380
8 Ramsteiner, F. and Heckmann, W. *Polymer* 1985, **26**, 199
9 Muratoglu, O. K., Argon, A. S. and Cohen, R. E. *Polymer* In press
10 Lin, L. and Argon, A. S. *Macromolecules* 1992, **25**, 4011
11 Wilson, F. C. in 'Materials Research Society Symposium Proceedings', MRS, Boston, MA, 1989, p. 413
12 Martinez-Salazar, J. and Cannon, C. G. *J. Mater. Sci. Lett.* 1984, **3**, 693
13 Lin, L. *PhD Thesis* Massachusetts Institute of Technology, 1991
14 Galeski, A., Argon, A. S. and Cohen, R. E. *Macromolecules* 1988, **21**, 2761
15 Atkins, E. Personal communication, 1994
16 Bartczak, Z., Argon, A. S. and Cohen, R. E. *Macromolecules* 1992, **25**, 5036
17 Ban, L. L., Doyle, M. J., Disko, M. M. and Smith, G. R. *Polym. Commun.* 1988, **29**, 163
18 Borggreve, R. J. M. and Gaymans, R. J. *Polymer* 1989, **30**, 63